$(\alpha,2\alpha)$ cluster knockout reaction on ^{9}Be and ^{12}C at 580 MeV

A. Nadasen, J. Brusoe, J. Farhat, K. A. G. Rao, D. Sisan, and J. Williams
Department of Natural Sciences, University of Michigan, Dearborn, Michigan 48128

P. G. Roos, F. Adimi,* T. Gu,† and M. Khayat‡
Department of Physics, University of Maryland, College Park, Maryland 20742

R. E. Warner
Department of Physics, Oberlin College, Oberlin, Ohio 44074
(Received 1 September 1998)

Cross-section measurements of the ^{9}Be,^{12}C$(\alpha,2\alpha)$ reaction at 580 MeV bombarding energy are presented. The data are compared with distorted-wave impulse approximation calculations. The agreement between theory and experiment suggests a dominance of the quasifree knockout mechanism. The extracted α-particle spectroscopic factors are in reasonable agreement with theory and proton-induced knockout reactions, unlike measurements for the $(\alpha,2\alpha)$ reaction at energies $\leqslant$140 MeV, but still show significant angular dependence. [S0556-2813(99)04302-2]

PACS number(s): 21.60.Gx, 24.10.Eq, 25.55.−e

I. INTRODUCTION

The clustering of α particles in nuclei has been studied for several decades. The first extensive work was carried out with transfer reactions [1–3]. Using distorted-wave Born approximation calculations, relative spectroscopic factors were determined for a number of nuclei spanning the periodic table. Subsequently, data from proton-induced α-particle knockout [4–8] reactions, analyzed with distorted-wave impulse approximation (DWIA) calculations, were used to obtain absolute spectroscopic factors for selected *p*-shell and *s-d* shell nuclei. These two types of reactions are complementary in that they probe rather different regions of momentum transfer to the residual nucleus, and thus different momenta of the struck α cluster. Transfer reactions, particularly at the higher energies, sample the high momentum components of the α cluster. On the other hand, the flexibility of the three-body final-state kinematics permits one to sample the lowest momenta of the struck α cluster using knockout reactions.

The use of composite projectiles to induce knockout reactions initially led to contradictory results. Even for the tightly bound α-particle projectile, problems were encountered. In the 90 MeV [9] and 140 MeV [10] $(\alpha,2\alpha)$ studies, spectroscopic factors obtained using DWIA calculations with standard geometrical parametrizations for the α-cluster bound state were two orders of magnitude larger than those obtained with incident protons or those from shell-model theoretical predictions. This discrepancy in the α-induced reaction necessitated the use of very large radii for the α bound-state potential geometry to reduce the spectroscopic factors to values comparable to those obtained from proton-induced reactions. The need for such large bound-state radii has been interpreted [10] as indicating excessive clustering in the low-density tail region of the nucleus. This clustering at large radii could result from either nuclear structure effects or an induced polarization of the nucleus by the α projectile.

However, $(\alpha,2\alpha)$ results at 197 MeV [11] and very limited data at 850 MeV [12] seem to contradict the lower energy studies in that both claim to obtain acceptable spectroscopic factors with standard bound α-cluster geometrical parametrizations. This energy dependence of the reaction warrants further investigation. Therefore, we have studied the $(\alpha,2\alpha)$ cluster knockout reaction at 580 MeV, and report in this manuscript our results for the *p*-shell nuclei ^{9}Be and ^{12}C.

Section II describes the experimental procedure. The experimental results of the measurements are given in Sec. III. The DWIA analyses and the deduced spectroscopic factors are discussed in Sec. IV, and a summary of our results and conclusions are presented in Sec. V.

II. EXPERIMENTAL PROCEDURE

The experiment was carried out at the National Superconducting Cyclotron Laboratory of Michigan State University. Beams of 580 MeV α particles were produced by the K1200 cyclotron and momentum analyzed with the two dipoles of the A1200 analyzing system. The beam energy was measured to approximately 1%, and had an energy spread of about 0.1%. The beam-line elements were adjusted for minimal steering of the beam by the focusing quadrupoles and produced a beam spot on target 2 mm wide by 4 mm high.

The beam traveled along the axis of a cylindrical scattering chamber, 2.3 m in diameter and 3.0 m long. Self-supporting natural targets of 8.9 mg/cm^2 C (99% ^{12}C) and 4.83 mg/cm^2 ^{9}Be were mounted at the center of the chamber. The total beam charge for each run was collected in a Faraday Cup located downstream from the chamber and integrated with a current integrator.

*Present address: Research and Data Systems Corporation, 7833 Walker Dr., Suite 550, Greenbelt, MD 20770.

†Present address: Cable & Wireless USA, 1919 Gallows Road, Vienna, VA 22182.

‡Present address: Research and Data Systems Corporation, 7833 Walker Dr., Suite 550, Greenbelt, MD 20770.

The detection systems were mounted on an arm (for left-hand measurements) and a table (right-hand measurements), both rotatable about an axis through the target center. Three telescopes with 10° separation were mounted on the arm, and were paired with three similar telescopes on the table. All telescopes were accurately adjusted with the aid of an optical transit to be in the same horizontal plane as the target center. Each telescope consisted of a collimator (3.0 cm thick brass with a 1.9 cm diameter circular aperture) followed by a 1.0 mm thick ΔE Si surface barrier detector (450 m^2 active area) and a 5 cm diameter by 7.5 cm thick E NaI(Tl) detector. The detectors were capable of stopping all α particles of interest. Signals from the detectors were sent through-charge sensitive preamplifiers to the data acquisition area.

For each telescope $\Delta E-E$ fast coincidences were made. The two-dimensional energy spectra of these signals provided clean separation between α particles and all other particles incident on the telescope. Additional coincidences were formed pairwise between the telescopes on the arm and those on the table. In particular a coincidence was obtained between the smallest angle telescope on the arm (Tel 1) and the largest angle telescope (Tel 6) on the table. Similarly, coincidences were required for Tel 2 with Tel 5, and Tel 3 with Tel 4. The system thus allowed concurrent measurements at three angle pairs with equal-included angles. These coincidences were formed using time-to-digital converters (TDC's) and had a time resolutions of 5–10 ns, which was sufficient to separate individual rf beam bursts. The TDC range of 200 ns permitted simultaneous accumulation of real and random coincidences. The firing of any of the three telescope pairs listed above constituted an event. The solid angles subtended by the forward telescopes of each pair were chosen to compensate for the variation in cross section with angle. Thus the solid angles were 0.56, 1.4, and 3.2 msr for telescopes 1, 2, and 3, respectively.

Pulser signals generated at a rate proportional to the beam current were sent to all preamplifiers and processed together with the real detector events. These signals were used to correct for gain shifts in the detectors and loss of events due to deadtime of the electronics and the computer data acquisition. The Si detectors were calibrated using a ^{228}Th α source. The NaI detectors were calibrated using α elastic scattering from a Au target. The accuracy of angular positioning of the detectors was determined by measuring coincidences from $\alpha+d$ elastic scattering using a CD_2 target.

All data were written event-by-event to magnetic tapes for detailed off-line analyses. During the experiment, one- and two-dimensional arrays of data were created for on-line monitoring of particle identification, detector gains, random rates, dead times, and statistics. Runs were usually limited to 2 h in order to facilitate corrections for gain drifts of the detectors.

III. EXPERIMENTAL RESULTS

The $(\alpha,2\alpha)$ reaction yields were measured at six quasifree angle pairs for ^{9}Be and three quasifree angle pairs for ^{12}C; i.e., angle pairs for which zero recoil momentum of the residual nucleus is allowed. The forward α angle for the ^{9}Be data ranged from 15° to 40° in steps of 5°. Those for ^{12}C were 15°, 25°, and 35°.

During replay, α particles were identified for each telescope by placing a window in the two-dimensional $\Delta E-E$ particle identification spectra. Further gates on TDC spectra of pairs of telescopes were used to reject random coincidences. For each angle pair, a two-dimensional spectrum of α energies of the two telescopes was created. A calculated kinematic locus ($E1$ vs $E2$) projected onto the coincidence two-dimensional α-energy spectrum indicated the region for $(\alpha,2\alpha)$ knockout events leading to the ground state of the residual nucleus. These events gave the highest combined energy of the two α particles and were cleanly separated from other α-α coincidences. They were then projected onto the energy axis of the smaller angle telescope, resulting in an energy-sharing distribution.

The measured energy-sharing cross sections for ^{9}Be are shown in Fig. 1 and those for ^{12}C in Fig. 2. The errors on the data points reflect statistical errors only. Relative errors from other sources are estimated to be less than 3% and have not been included in the analysis. Absolute errors in the cross-section data are estimated to be less than 10%. Each energy-sharing spectrum is characterized by a smooth broad distribution reaching a maximum near the energy corresponding to zero recoil momentum for the residual nucleus (denoted by an arrow on the abscissa), indicating dominance of quasifree α-cluster knockout. (We believe the excessively broad structure of the quasifree peak for ^{9}Be at 20° arises from a gain shift in the NaI detector during data taking. The detailed shape of the peak for this angle pair should therefore be ignored, but the integrated yield for the peak is correct.) The angular dependence of the peak energy and cross section is expected to correspond to that of free α-α elastic scattering. This is clearly demonstrated for the energy, as the energy of the peak shifts downward with increasing angle according to α-α kinematics. The angular dependence of the energy integrated $(\alpha,2\alpha)$ cross section as a function of the α-α center-of-mass angle is shown in Fig. 3. Also shown are elastic α-α cross sections at 620 MeV [13] as a solid line connecting the data points. The $(\alpha,2\alpha)$ data have been arbitrarily normalized to the elastic-scattering data. It is clear that the trend of the knockout data is quite consistent with α-α elastic scattering at nearly the same energy.

A comparison of the ^{12}C and ^{9}Be data for the same α-particle angles shows that the peak cross sections for ^{12}C are roughly a factor of 5 smaller than those for ^{9}Be. This decrease with increasing target mass is common for quasifree knockout reactions and has been observed in other α-cluster knockout investigations [6,10]. The distributions for both target nuclei are asymmetric, falling more slowly on the low-energy side of the quasifree peaks. The distributions for ^{12}C appear to be slightly broader, probably reflecting the larger α-particle separation energy. There is also the possibility of broadening due to contributions from the knockout of an $L=2$ α cluster. For ^{12}C the transition is dominated by an $L=0$ transition (there is a small $L=2$ contribution due to the 2^+ state in ^{8}Be which is unresolved from the ground state in the present experiment), whereas for ^{9}Be contributions from both $L=0$ and $L=2$ are expected. Since the $L=2$ distribution has a minimum at zero recoil momentum and peaks at momenta of approximately ± 125 MeV/c, the $L=2$ contributions broaden the distribution. However, as we shall see in the next section the $L=2$ contributions are predicted to be small for the quasifree angles.

IV. ANALYSIS

A. DWIA formalism

The data were compared with predictions of the distorted-wave impulse approximation (DWIA) using the code THREEDEE [14]. In the DWIA the triple differential cross section for the reaction $A(\alpha,2\alpha)B$ resulting in the knockout of an α particle with orbital angular momentum L (projection λ) is given by

$$\frac{d^3\sigma}{d\Omega_1 d\Omega_2 dE_1} = KS_L \frac{d\sigma}{d\Omega_{\alpha-\alpha}} \sum_{\lambda} |T_{BA}^{L\lambda}|^2 \tag{1}$$

where K is a well-defined kinematic factor, S_L is the cluster spectroscopic factor for a specific L, and $d\sigma/(d\Omega_{\alpha-\alpha})$ is the two-body half-off-the-energy-shell α-α cross section. The quantity $T_{BA}^{L\lambda}$ is often referred to as the distorted momentum distribution, since in the plane-wave limit it is proportional to the momentum space wave function of the bound α cluster. It can be written as

$$T_{BA}^{L\lambda} = (2L+1)^{-1/2} \int \chi_2^{(-)*}(\mathbf{r}) \chi_1^{(-)*}(\mathbf{r}) \phi_{L\lambda}^{\alpha}(\mathbf{r}) \chi_0^{(+)}(\gamma\mathbf{r}) d\mathbf{r} \tag{2}$$

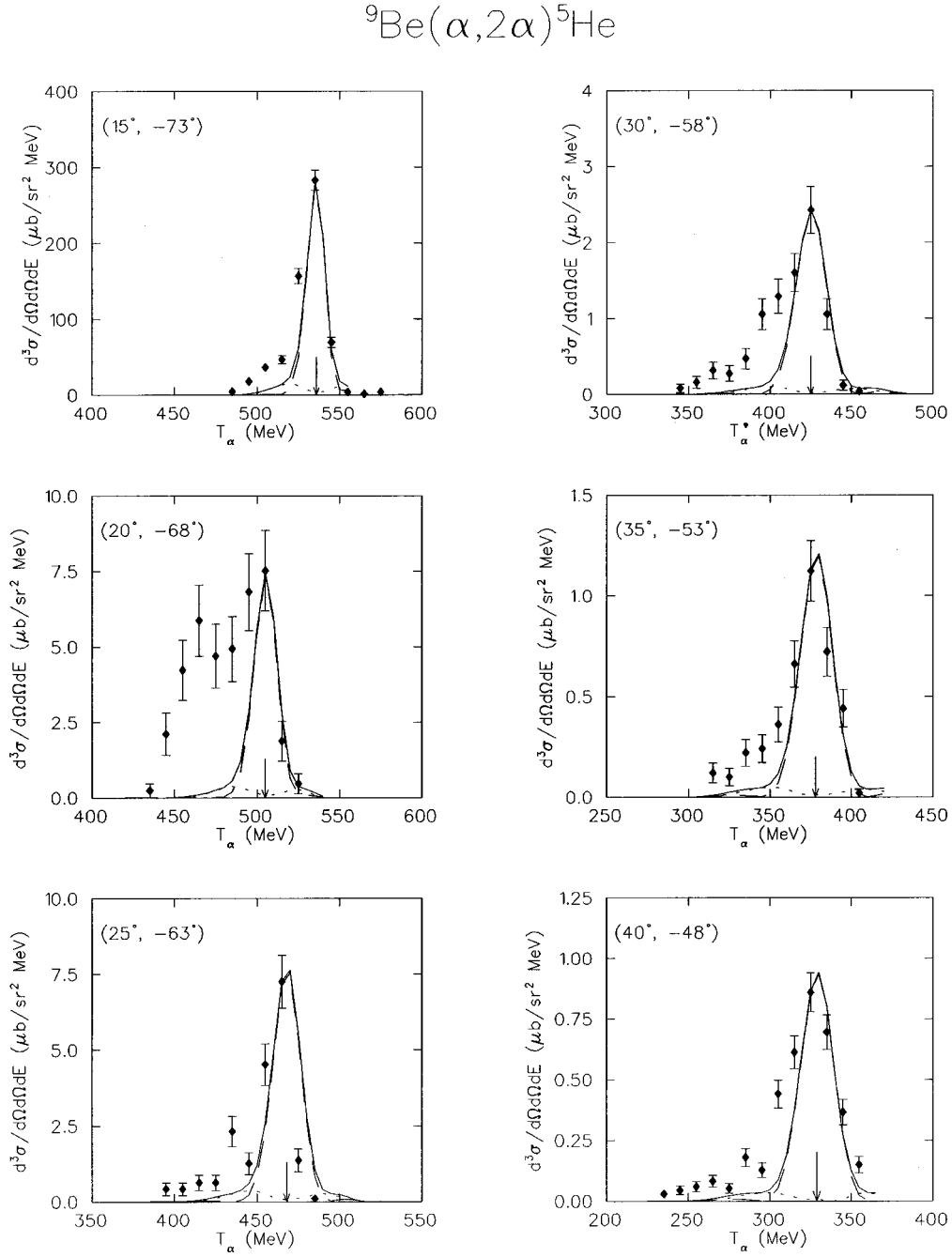

FIG. 1. Energy-sharing cross sections for the ^{9}Be$(\alpha,2\alpha)^5$He reaction at 580 MeV. The emitted α-particle quasifree angle pairs are indicated in the figures. The curves represent DWIA calculations for $L=0$ (dashed), $L=2$ (dotted), and their incoherent sum (solid) normalized to the data. The arrow on the x axis indicates the location for which the residual nucleus has zero recoil momentum.

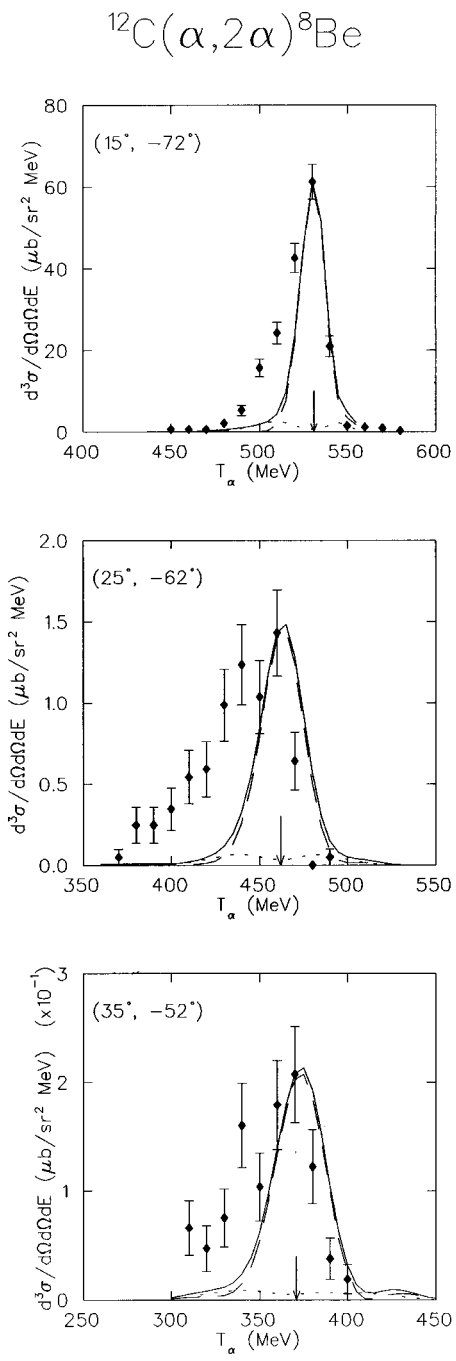

FIG. 2. Energy-sharing cross sections for the ^{12}C(α,2α)^{8}Be reaction at 580 MeV. The emitted α-particle quasifree angle pairs are indicated in the figures. The curves represent DWIA calculations for $L=0$ (dashed), $L=2$ (dotted), and their incoherent sum (solid) normalized to the data. The arrow on the x axis indicates the location for which the residual nucleus has zero recoil momentum.

where the $\chi^{(+)}$ and $\chi^{(-)}$ represent the distorted waves for the incoming and outgoing α particles, respectively. These are generated using optical model parameters derived from α-nucleus elastic-scattering data. The ratio B/A of the masses of the residual and target nuclei is denoted by γ. The quantity $\phi^{\alpha}_{L\Lambda}$ is the ''bound-state wave function'' of the α cluster in the target nucleus.

As is customary in most DWIA analyses, the two-body half-off-the-energy-shell α-α cross section is replaced by a nearby on-shell cross section. At this high energy we expect the off-shell effects to be small. There are a variety of prescriptions for the choice of on-shell point, and we have chosen to use the final-energy prescription (FEP). In this prescription the α-α center-of-mass energy and angle are assumed to be those which give rise to the final-state α-α system measured in the (α,2α) reaction. An alternative method would be the initial energy prescription in which the α-α kinematics are chosen to be consistent with the initial state of the incident and bound α clusters. For these two prescriptions the calculated on-shell α-α angles are identical and the on-shell α laboratory energy differs by only about 15 MeV for the worst case of ^{12}C. This would lead to approximately a 20% change in the two-body cross section used in the DWIA calculations, a relatively small difference compared to other uncertainties in the calculations. With the choice of the FEP for the on-shell kinematic prescription we obtained the two-body α-α cross sections at the appropriate energy and angle from an interpolation of the available α-α elastic scattering data in the energy range from 100 to 620 MeV.

Equation (1) represents a factorized impulse approximation in which the two-body cross section enters as a multiplicative factor rather than a t-matrix for the α-α interaction. It is important to verify that this factorization approximation is indeed valid. Explicit DWIA calculations show that $T^{L\Lambda}_{BA}$ varies by less than 10% at zero recoil momentum over the angular range of the present measurements. In addition the kinematic factor K varies more slowly and is calculable. Therefore, the angular dependence of the triple differential cross section [Eq. (1)] is primarily due to $d\sigma/d\Omega_{\alpha-\alpha}$. The agreement between the energy-integrated (α,2α) cross sections and the elastic $d\sigma/d\Omega_{\alpha-\alpha}$ presented in Fig. 3 lends strong support for the use of the factorization approximation in the DWIA calculations.

B. Optical model potentials

The optical model potential parameters used to calculate the distorted waves for the incident and emitted α particles

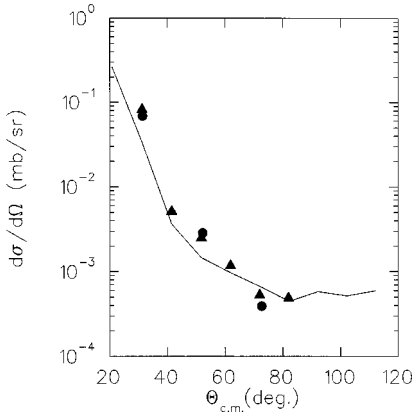

FIG. 3. The α-α elastic-scattering differential cross section at 620 MeV. The solid line simply connects the data points. The solid triangles are the integrated cross sections of the ^{9}Be(α,2α)^{5}He data presented in Fig. 1, normalized to the elastic data with one overall normalization. The solid circles are the integrated cross sections of the ^{12}C(α,2α)^{8}Be data presented in Fig. 2, normalized to the elastic data with one overall normalization.

were derived from systematic analyses of existing α-nucleus optical model potentials. Using potentials for light nuclei at energies of 104 [15], 139 [16], 166 [17], and 172 [18] MeV and for heavier nuclei at energies from 288 to 699 MeV [19], both the energy and the target mass dependence of the α-nucleus potential parameters were derived.

Initially the volume integrals per nucleon-nucleon pair ($J/4A$) of the real and imaginary optical model potentials were calculated from the lowest energy up to 699 MeV. These were plotted as a function of beam energy. For the real volume integral, data above 100 MeV clearly indicated a logarithmic dependence on the bombarding energy. This energy dependence was well described by $J_R/4A = J_0 - \beta \ln E$ with $J_0 = 964$ MeV fm^3 and $\beta = 124$ MeV fm^3. The magnitude and energy dependence are consistent with those from the optical model analyses of elastic scattering of other light ions [8,20,21]. When the derived energy dependence was extrapolated to lower energies, where there exist a variety of ambiguities in the optical model potentials, it was found that several empirical potentials were in agreement with our derived energy dependence. In addition we found that the target mass dependence of the volume integrals was very weak. Therefore, for the real potentials we fixed the radius parameter at 1.22 fm and the diffuseness parameter at 0.76 fm, and calculated the strengths of the real potentials necessary for the DWIA analysis.

The volume integrals for the imaginary potentials showed an initial rise with α-particle bombarding energy up to approximately 90 MeV, followed by a slow decrease to 140 MeV and then a gradual rise to 699 MeV. Again the target mass dependence of the volume integral was weak. Therefore, using radius and diffuseness parameters of 1.6 and 0.6 fm, respectively, the strengths of the imaginary potentials for the various energies and masses were calculated.

Since each energy-sharing distribution contains a range of α-particle energies, an attempt was made to include the energy dependence of the optical model potentials across the energy-sharing distribution. However, due to the narrow range of energies in the distribution, these DWIA calculations did not differ significantly from calculations using potentials at fixed energies. Therefore, for each energy-sharing distribution, calculations were carried out with fixed α-particle potentials corresponding to the energy at the minimum recoil momentum point.

To investigate the sensitivity of the DWIA calculations to the optical model parameters, calculations were carried out in which the input parameters were varied. A variation of the strengths of each of the α-particle optical model potentials by 20% produced essentially no change in the shape of the energy-sharing distribution. However, the overall magnitude of the peak cross section changed by about 5% for changes of 20% in the real potential strength, and by about 10% for changes in the imaginary potential strength. More sensitivity was exhibited for variations in the bound-state potential geometry. A 20% variation in the radius parameter or the diffuseness produced about a 25% change in the peak cross section. Overall one might expect up to a factor of 2 variation in the cross sections resulting from uncertainties in the optical model parameters and bound-state geometry.

The final optical model parameters used in the DWIA analysis of the present data are presented in Table I.

TABLE I. Optical model potential parameters for the α-particle scattering wave functions. The potential is of the form: $-U(r) = V/(1+e^x) + \imath W/(1+e^{x'}) - U_{\rm coul}(R_C)$, where $x = (r - r_0 A^{1/3})/a$, and $x' = (r - r_0' A^{1/3})/a_0'$. The quantity $U_{\rm coul}(R_C)$ is the Coulomb potential due to a sphere of the charge of radius $R_C = 1.3A^{1/3}$. As described in the text the geometrical parameter were fixed at the values $r_0 = 1.22$ fm, $a_0 = 0.76$ fm, $r_0' = 1.6$ fm, and $a_0' = 0.60$ fm. The strengths of the potentials for the incident (subscript 0) and emitted (subscripts 1 and 2) α particles are listed in the table.

		Potential strengths (MeV)					
	$\Theta_1/-\Theta_2$	V_0	V_1	V_2	W_0	W_1	W_2
^{12}C	15°/72°	52.8	41.1	99.3	18.8	18.8	17.9
^{12}C	25°/62°	52.8	45.3	81.5	18.8	17.8	15.3
^{12}C	35°/52°	52.8	51.9	68.2	18.8	17.6	16.3
^{9}Be	15°/73°	48.4	34.8	64.8	17.7	16.8	16.0
^{9}Be	20°/68°	48.4	36.6	67.0	17.7	16.5	15.0
^{9}Be	25°/62°	48.4	38.3	69.0	17.7	16.3	14.0
^{9}Be	15°/73°	48.4	41.1	63.3	17.7	16.0	14.3
^{9}Be	20°/68°	48.4	44.0	57.6	17.7	15.7	14.6
^{9}Be	25°/62°	48.4	46.9	51.9	17.7	15.4	14.9

C. Bound cluster wave function

The bound α-cluster wave functions $\phi^{\alpha}_{L\Lambda}$ used in the DWIA calculations were taken to be eigenstates of an α-particle bound in a Woods-Saxon potential with a binding energy equal to the α-particle separation energy. For comparison with previous experiments we have taken the geometrical parameters of the potential from Refs. [5,8,11]. As in these references the quantum numbers were chosen to be those corresponding to a harmonic-oscillator shell model; i.e., for these $1p$-shell nuclei the quantum numbers (N,L) are $3S$ for $L=0$ transitions and 2D for $L=2$ transitions.

D. Results of the DWIA calculations

The calculated energy-sharing distributions are presented in Figs. 1 and 2. For ^{9}Be the dashed lines are the DWIA calculations for the knockout of a $3S\alpha$ cluster, and the dotted lines are for the knockout of a 2D cluster. The solid lines are their incoherent sum. All calculations have been normalized to the peak cross section with the spectroscopic factors shown in Table II. It is clear that the calculated energy-sharing distributions are significantly narrower than the data. The enhancement of the experimental cross sections on the lower energy side of the energy-sharing distributions relative to the DWIA calculations was also observed at lower energies. At lower bombarding energies [10] the authors have suggested that the enhancement is due to the excitation of the target nucleus to excited states with large α-particle parentage which decay by α emission. Such transitions cannot be kinematically separated from the direct α knockout reaction. In the present experiment, due to the high energy of the incident α particles, such an explanation seems unlikely. Even at the smallest angles one would require a state at an excitation energy greater than 40 MeV to produce contributions on the low-energy side of the quasifree peak.

For the ^{12}C$(\alpha,2\alpha)^{8}$Be reaction to the ground state, only an $L=0$ transition is possible. The dashed lines in Fig. 2

TABLE II. Spectroscopic factors extracted from normalization of the DWIA calculations to the peak of the energy-sharing distribution.

Target	Θ_1/Θ_2	S_L
^{12}C	15°/−72°	4.1
^{12}C	25°/−62°	1.9
^{12}C	35°/−52°	0.55
^{9}Be	15°/−73°	2.0
^{9}Be	20°/−68°	(a)
^{9}Be	25°/−63°	1.0
^{9}Be	30°/−58°	0.46
^{9}Be	35°/−53°	0.58
^{9}Be	40°/−48°	0.37

[a]Energy-sharing distribution effected by a gain shift.

show these calculations. However, due to our limited energy resolution, events leading to the 2^+ state of ^{8}Be at 2.9 MeV cannot be separated. Our data thus include transitions to both the ground state and the first excited state. Therefore, we also made calculations for transitions to the first excited state, normalized using the spectroscopic factors predicted by the shell-model calculations. These are shown as dotted lines in Fig. 2. Clearly for these quasifree angle pairs the $L=2$ contribution is very small. As with the ^{9}Be data we observed excess enhancement on the low-energy side of the energy-sharing distributions.

Although we have already pointed out that the $(\alpha,2\alpha)$ data generally follow the angular dependence of the α-α elastic-scattering data, the details show significant deviation. From Table II we note that the spectroscopic factors range from 0.4 to 2.0 for ^{9}Be and from 0.6 to 4.1 for ^{12}C. This variation is not related to uncertainties in the data. However, uncertainties in the input parameters for the calculations could result in differences on the order of a factor of two. Of particular concern are the large values obtained at the forward angles compared to those at larger angles. Since at this forward angle the α-α impact parameter is large, polarization of the target nucleus by the incident α particle followed by the knockout of the α cluster at a large radius is still a concern. In fact, this was suggested as a possible explanation for the need to use very large bound-state radii in the DWIA analysis of the 140 MeV data [10]. To examine this question further we carried out a series of DWIA calculations to examine the radial localization of the $(\alpha,2\alpha)$ reaction at our energy of 580 MeV. In Fig. 4 we present the differences in DWIA cross section between calculations with radial cutoffs that differ by 0.5 fm. This has been shown to be a rather good indicator of the radial localization of various knockout reactions [6]. As can be seen, the radial localization at 15° (solid line) is essentially identical to that at 35° (dashed line). The localization is also nearly the same as that found at 190 MeV [11]. Thus such an explanation of the enhanced yield will not explain the difference between the forward angle and large angle data.

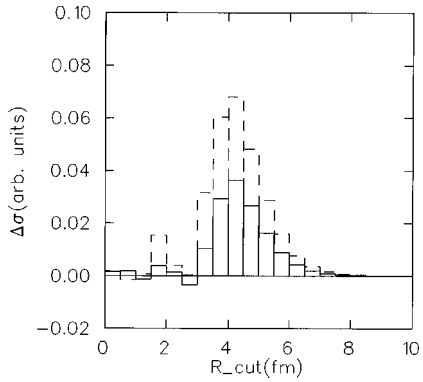

FIG. 4. Histograms of the change in cross section for ^{12}C$(\alpha,2\alpha)^8$Be as a function of cutoff radius for the angle pairs 15°/−72° (solid lines) and 35°/−52° (dashed lines). The quantity $\Delta\sigma=\sigma(R_{\rm cut}+0.5)-\sigma(R_{\rm cut})$ and $R_{\rm cut}$ is the cutoff radius used in a series of DWIA calculations.

V. SUMMARY AND CONCLUSIONS

We have measured the $(\alpha,2\alpha)$ knockout reaction cross sections at six quasifree angle pairs for ^{9}Be and three quasifree angle pairs for ^{12}C. These energy-sharing distributions show a prominent peak at zero momentum for the unobserved residual nucleus, which is evidence for the dominance of a quasifree knockout of an $L=0$ α cluster in the reaction.

The data have been compared with DWIA calculations of cluster knockout. We find that the widths of experimental energy-sharing distributions, which should reflect the range of momenta of the α cluster in the target nucleus, to be broader than those predicted by DWIA. The experimental distributions correspond to momentum distributions with a full width at half maximum of about 130 MeV/c. This value is in qualitative agreement with results at lower energies and other methods of determining the momentum distribution.

The spectroscopic factors obtained from the DWIA analysis of the data exhibit fairly strong angular dependence, varying by a factor of 5 over the angular range of the ^{9}Be data, and a factor of 7 for ^{12}C. The largest spectroscopic factors arise from the forward angle data. At these angles the α-α impact parameters are large, and one might expect the knockout reaction to take place at larger radii where enhanced clustering or coupled channel effects might occur. To examine the effects we followed the procedure of Ref. [10] and carried out calculations for ^{12}C using a larger bound-state radius, increasing the radius parameter from the nominal value of 1.35–2.70 fm. This change did not have as profound an effect as at 140 MeV. The magnitude of the cross section is less sensitive to the bound-state radius at 580 MeV. Doubling the radius parameter reduced the spectroscopic factor at 15° by roughly a factor of 3, but also reduced the spectroscopic factors at other angle pairs by a comparable amount. Thus an increased radius would not correct the angular dependence of the spectroscopic factors. We note that a similar enhancement of the forward angle cross section is observed at 190 MeV [11].

In spite of the difficulties at forward angles, the values of the spectroscopic factors resulting from the larger angle data are in rather good agreement with the theoretical predictions [2] and $(p,p\alpha)$ studies [6]. This is in contrast with results at 90 [9] and 140 MeV [10] where much larger spectroscopic factors were obtained with the same bound-state geometry, even for the large angles. Clearly the results at 90 and 140 MeV have a deficiency that does not exist in the present

investigation. Those results may reflect either an inability of the DWIA to account for the large distortions present at such low energies or a real physical phenomenon such as polarization of the nucleus by the incident α particles. Such polarization may be more serious, the lower the velocity of the projectile α particle. Our results are in reasonable agreement with those at 190 and 850 MeV, an indication that for energies of 190 MeV and higher, the $(\alpha,2\alpha)$ reaction is becoming a useful tool for the investigation of α clusters in nuclei. Energies of 140 MeV and below appear to be too low for the $(\alpha,2\alpha)$ reaction to provide any reasonable nuclear structure information.

These results suggest a transition in the dynamics of the $(\alpha,2\alpha)$ reaction between 140 and 190 MeV; i.e., in the 35 to 50 MeV/nucleon region. The reason for this dramatic change over such a small energy range is not clear. However, we note that other reactions have shown some evidence for a transition in this energy range. For example, a transition from sequential decay to instantaneous multifragmentation has been observed for heavy-ion reactions in this same energy range [22]. This has been interpreted as a saturation of the energy deposition in a nuclear system, the higher energy densities leading to rapid expulsion of the particles. Also a study of nucleon-induced reactions noted a significant change in the distribution of particle emission around 40 MeV [23]. At low energies evaporation products dominate the emission spectra. Above 40 MeV a significant enhancement of pre-equilibrium particles is observed. This may be envisaged as the creation of small hot spots by the projectile, leading to early expulsion of high-energy particles. Presumably this could be related to the properties of the fundamental nuclear forces. At low energies the attractive nuclear mean field is the major force, and at high energies the nucleon-nucleon force dominates. One may speculate that the onset of dominance of individual nucleon-nucleon interactions over nucleus-nucleus collisions occurs in the 35–50 MeV energy region. If true, this same concept would apply to the $(\alpha,2\alpha)$ reaction which we are treating within the DWIA, assuming the dominance of nucleon-nucleon collisions. At the lower energies of 35 MeV/nucleon the mean-field effects must dominate, leading to poor agreement between experiment and DWIA theory. Further studies are needed to understand the transition in this energy range.

ACKNOWLEDGMENTS

We thank the NSCL operations staff for providing the excellent beams of α particles. This work was supported in part by the National Science Foundation under Grants No. PHY-9602869 (UM-Dearborn), PHY-9513924 (UMd), and PHY-9423659 (Oberlin College).

[1] G. J. Wozniak, D. P. Stahel, J. Cerny, and W. A. Jelley, Phys. Rev. C **14**, 815 (1976).
[2] N. Anantaraman, C. L. Bennet, J. P. Draayer, H. W. Fulbright, H. E. Gove, and J. Toke, Phys. Rev. Lett. **35**, 1131 (1975).
[3] H. Yoshida, Phys. Lett. **47B**, 411 (1973).
[4] D. Bachelier, M. Bernas, O. M. Bilaniuk, J. L. Boyard, J. C. Jourdain, and P. Radvanyi, Phys. Rev. C **7**, 165 (1973).
[5] P. G. Roos, N. S. Chant, A. A. Cowley, D. A. Goldberg, H. D. Holmgren, and R. Woody III, Phys. Rev. C **15**, 69 (1977).
[6] T. A. Carey, P. G. Roos, N. S. Chant, A. Nadasen, and H. L. Chen, Phys. Rev. C **29**, 1273 (1984).
[7] A. Nadasen *et al.*, Phys. Rev. C **39**, 536 (1989); A. Nadasen *et al.*, *ibid.* **47**, 674 (1993).
[8] A. Nadasen, P. G. Roos, N. S. Chant, C. C. Chang, G. Ciangaru, H. F. Breuer, J. Wesick, and E. Norbeck, Phys. Rev. C **40**, 1130 (1989).
[9] J. D. Sherman, D. L. Hendrie, and M. S. Zisman, Phys. Rev. C **13**, 20 (1976).
[10] C. W. Wang, N. S. Chant, P. G. Roos, , and T. A. Carey, Phys. Rev. C **21**, 1705 (1980).
[11] A. A. Cowley, G. F. Steyn, S. V. Fortsch, J. J. Laurie, J. V. Pilcher, G. D. Smit, and D. M. Whittal, Phys. Rev. C **50**, 2449 (1994).
[12] N. Chirapatpimor *et al.*, Nucl. Phys. **A264**, 379 (1976).
[13] A. Nadasen (unpublished).
[14] N. S. Chant and P. G. Roos, Phys. Rev. C **15**, 57 (1977).
[15] B. Hauser, R. Dohkin, H. Rebel, G. Schatz, G. W. Schweimer, and J. Specht, Nucl. Phys. **A128**, 81 (1969).
[16] S. M. Smith, G. Tibell, A. A. Cowley, D. A. Goldberg, H. G. Pugh, W. Reichart, and N. S. Wall, Nucl. Phys. **A207**, 273 (1973).
[17] B. Tatischeff and I. Brissaud, Nucl. Phys. **A155**, 89 (1970).
[18] A. Kiss, C. Mayer-Boricke, M. Rogge, P. Turek, and S. Wiktor, J. Phys. G **13**, 1067 (1987).
[19] B. Bonin *et al.*, Nucl. Phys. **A445**, 381 (1985).
[20] A. Nadasen, P. Schwandt, P. P. Singh, W. W. Jacobs, A. D. Bacher, P. T. Debevec, M. D. Kaitchuck, and J. Meek, Phys. Rev. C **23**, 1023 (1981); P. Schwandt, in *Proceedings of the Workshop on the Interactions between Medium Energy Nucleons in Nuclei*, AIP Conf. Proc. No. 97, edited by H. O. Meyer (AIP, New York, 1982), p. 89.
[21] A. Nadasen, P. G. Roos, N. S. Chant, C. C. Chang, and T. A. Carey, Bull. Am. Phys. Soc. **26**, 580 (1981); A. Nadasen and P. G. Roos, *ibid.*, **26**, 1040 (1984.
[22] D. A. Cebra, S. Howden, J. Karn, A. Nadasen, C. A. Ogilvie, A. van der Molen, G. D. Westfall, W. K. Wilson, J. S. Winfield, and E. Norbeck, Phys. Rev. Lett. **64**, 2246 (1990); W. J. Llope *et al.*, Phys. Rev. C **52**, 1900 (1995).
[23] J. R. Wu, C. C. Chang, and H. D. Holmgren, Phys. Rev. C **19**, 698 (1979); **19**, 370 (1979); **19**, 659 (1979); A. A. Cowley, C. C. Chang, H. D. Holmgren, J. D. Silk, D. L. Hendrie, R. W. Koontz, P. G. Roos, C. Samanta, and J. R. Wu, Phys. Rev. Lett. **45**, 1930 (1980).